

# Taking Charge: Metal Ions Accelerate Amyloid Aggregation in Sequence Variants of $\alpha$ -Synuclein

Published as part of the Journal of the American Society for Mass Spectrometry virtual special issue "Focus: Neurodegenerative Disease Research".

Emily J. Byrd, Martin Wilkinson, Sheena E. Radford, and Frank Sobott\*



Cite This: *J. Am. Soc. Mass Spectrom.* 2023, 34, 493–504



Read Online

ACCESS |



Metrics & More

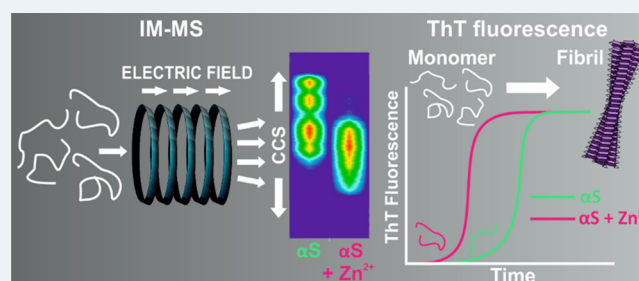


Article Recommendations



Supporting Information

**ABSTRACT:** Alpha-synuclein ( $\alpha$ S) is an intrinsically disordered protein which exhibits a high degree of conformational heterogeneity. *In vivo*,  $\alpha$ S experiences various environments which cause adaptation of its structural ensemble. Divalent metal ions are prominent in synaptic terminals where  $\alpha$ S is located and are thought to bind to the  $\alpha$ S C-terminal region. Herein, we used native nano-electrospray ionization ion mobility-mass spectrometry to investigate changes in the charge state distribution and collision cross sections of wild-type N-terminally acetylated (NTA)  $\alpha$ S, along with a deletion variant ( $\Delta\Delta$ NTA) which inhibits amyloid formation and a C-terminal truncated variant (119NTA) which increases the rate of amyloid formation. We also examine the effect of the addition of divalent metal ions,  $\text{Ca}^{2+}$ ,  $\text{Mn}^{2+}$ , and  $\text{Zn}^{2+}$ , and correlate the conformational properties of the  $\alpha$ S monomer with the ability to aggregate into amyloid, measured using Thioflavin T fluorescence and negative stain transmission electron microscopy. We find a correlation between the population of species with a low collision cross section and accelerated amyloid assembly kinetics, with the presence of metal ions resulting in protein compaction and causing  $\Delta\Delta$  to regain its ability to form an amyloid. The results portray how the  $\alpha$ S conformational ensemble is governed by specific intramolecular interactions that influence its amyloidogenic behavior.



## INTRODUCTION

The amyloid precursor protein alpha-synuclein ( $\alpha$ S) is structurally defined as an intrinsically disordered protein (IDP) and visits a large and diverse conformational space, including partially compact and extended states.<sup>1</sup> Aggregation and self-assembly of  $\alpha$ S into  $\beta$ -sheet rich amyloid fibril structures is associated with the onset of Parkinson's disease (PD) and other synucleopathies.<sup>2,3</sup> The neuropathology of PD is characterized by the deposition of insoluble cellular inclusions called Lewy Bodies (LB) in dopaminergic neurons in the substantia nigra of the brain.<sup>4,5</sup> The composition of LBs consists of fibrillar  $\alpha$ S, lipids, mitochondria, metal ions, and various other cellular components.<sup>6–8</sup> Monomeric  $\alpha$ S is found *in vivo* to partition between the cytoplasm and phospholipid membranes.<sup>9–11</sup> Although the exact functional role(s) of  $\alpha$ S remain uncertain, localization of  $\alpha$ S to presynaptic nerve terminals suggests a role in vesicle binding, clustering, and neurotransmitter release.<sup>12–15</sup> This proposed function relies on the lipid binding properties of  $\alpha$ S which are governed by the charge distribution across the protein sequence.<sup>16–18</sup>

The sequence of  $\alpha$ S is divided into three distinct regions: the N-terminal region which overall is positively charged (residues 1–60) containing imperfect KTKEGV repeats responsible for

lipid binding,<sup>16</sup> the nonamyloid- $\beta$  component (NAC) core (residues 61–95) which is hydrophobic and amyloidogenic, forming the core of  $\alpha$ S fibril polymorphs,<sup>19–23</sup> and the C-terminal region (residues 96–140) which contains 14 negatively charged residues at physiological pH responsible for binding dopamine, calcium, and other metal ions.<sup>24–26</sup>

The conformational freedom exhibited by  $\alpha$ S may play a role in its aggregation pathway, with different monomeric conformation families possessing different amyloid-forming potential.<sup>27</sup> Recently, Brodie et al. used cross-linking mass spectrometry (MS) and single molecule Förster resonance energy transfer (smFRET) guided molecular dynamics simulations to portray possible conformations of monomeric  $\alpha$ S.<sup>28</sup> Their findings identified the importance of inter-residue contacts between the N- and C-terminal regions for stabilizing conformations, proposing that a transient  $\beta$ -hairpin structure

**Received:** December 22, 2022

**Revised:** January 29, 2023

**Accepted:** February 3, 2023

**Published:** February 16, 2023



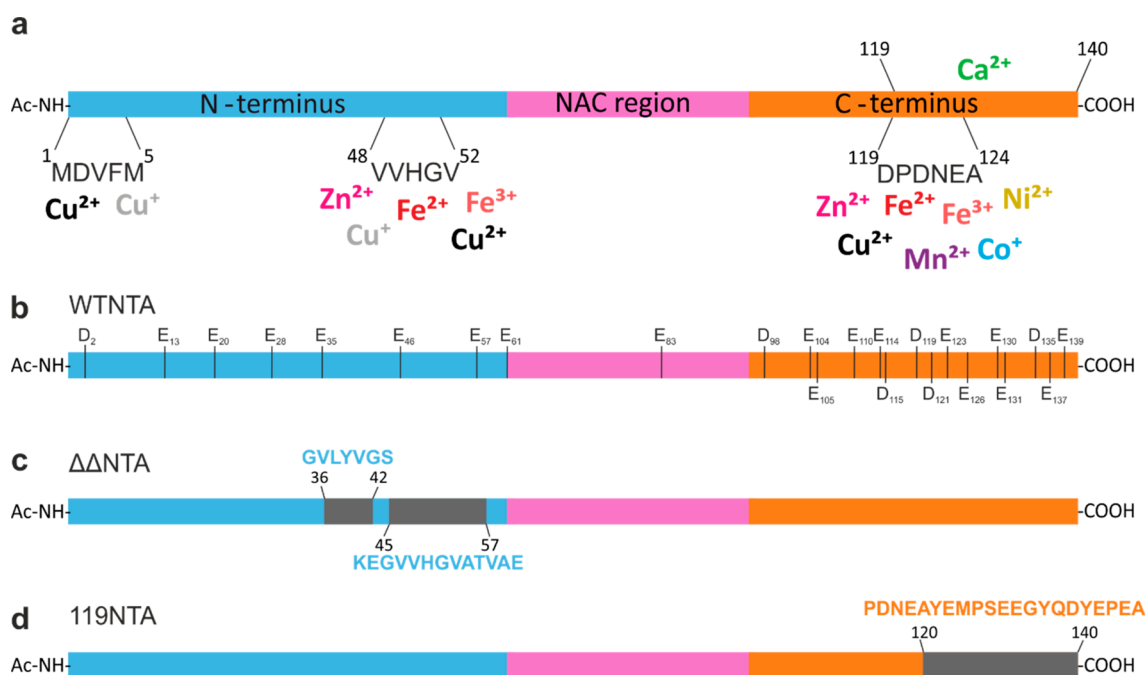


**Figure 1.**  $\alpha$ S is predicted to bind metal ions primarily in the negatively charged C-terminal region. (a) A range of monovalent, divalent, and trivalent metal ions are known to bind to negatively charged aspartic and glutamic acid residues that are enriched in the C-terminal region of  $\alpha$ S, with the binding sites mapped by NMR.<sup>24</sup> Some transition metals also interact with His50 and methionine residues in the N-terminal region.<sup>48</sup> (b) Full length sequence of WT NTA  $\alpha$ S acetylated at the N-terminus (denoted by Ac-NH) with each glutamic acid and aspartic acid residue labeled across the entire sequence. (c) Sequence of the  $\Delta\Delta$ -terminally acetylated  $\alpha$ S variant, the P1 and P2 regions, which are removed in this construct, are indicated by black boxes corresponding to residues 36–42 and 45–57, respectively. (d) Sequence of the C-terminal truncation variant cleaved at residue 119 in which residues 120–140 are deleted, as indicated by a black box. Variant 119 was also N-terminally acetylated in this study.

involving the NAC and C-terminal regions may form a nucleation site for early oligomers which could initiate the formation of the cross- $\beta$  structure of fibrils. Further to this, Chen et al. used these same smFRET data as an experimental restraint to guide discrete molecular dynamics (DMD) simulations in order to generate a snapshot of the  $\alpha$ S conformational ensemble.<sup>29</sup> They showed that the ensemble of monomeric  $\alpha$ S structures can be split into eight clusters distinguished by conformation, some of which exist within nanosecond and microsecond time scales. Transitions between conformations may follow a hierarchy of subpopulation dynamics, whereby some subpopulations may exist long enough to facilitate ligand binding. Specific subpopulations of monomeric  $\alpha$ S structures may preferably facilitate amyloid assembly and ultimately PD progression.

Oligomers that are believed to be toxic<sup>30</sup> and amyloid fibril structures of  $\alpha$ S are both composed primarily of  $\beta$ -sheets.<sup>31,32</sup> The adoption of specific structures under defined conditions infers that the roles of  $\alpha$ S, be they functional or pathological, might be a result of the precise conformational species of  $\alpha$ S monomers which can transition into  $\beta$ -sheet structures as oligomers assemble. Therefore, it is crucial to determine how the conformational ensemble of monomeric  $\alpha$ S and its sequence variants relates to their amyloid-forming potentials. Characterizing transient and heterogeneous species of IDPs, however, is experimentally challenging. Structural techniques such as nuclear magnetic resonance (NMR) rely on population averaging to visualize conformations in dynamic equilibrium with one another, which limits this technique in the number of states that it can discriminate.<sup>33</sup> Hence, the data output struggles to capture the structural fingerprints of species in a broad ensemble of interconverting states. Here, an integrative

approach using native nano-electrospray ionization (nESI) ion mobility-mass spectrometry (native IM-MS), measurement of the kinetics of amyloid formation using thioflavin T (ThT) fluorescence, and negative stain transmission electron microscopy (TEM) has been applied in order to capture the  $\alpha$ S conformational ensemble under different conditions and relate this fingerprint to its amyloid assembly kinetics.

Variants of  $\alpha$ S with deletions in the N-terminal region were recently created in order to identify regions within the 140 amino acid protein chain that could be important in controlling its amyloid formation propensity.<sup>34,35</sup> Doherty et al. used *in silico* analysis to identify two regions in the N-terminal region of  $\alpha$ S that exhibit predicted low solubility and high aggregation propensity. These regions include the seven residue sequence<sup>36</sup>GVLYVGS<sup>42</sup> named P1 and the 13 residue sequence<sup>45</sup>KEGVVHGVATVAE<sup>57</sup> named P2. Deleting P1 to create the  $\alpha$ S variant  $\Delta$ P1 inhibited aggregation into amyloid at physiological pH (pH 7.5) but not at acidic, lysosomal pH (pH 4.5). Deleting P2 alone ( $\Delta$ P2) had little effect on the half time ( $t_{50}$ ) of amyloid formation. However, deleting both P1 and P2 in tandem ( $\Delta\Delta$ ) abolished amyloid formation *in vitro* at both physiological and lysosomal pH within 100 h as shown by ThT fluorescence.<sup>34,35</sup> How these deletions control or abolish amyloid formation, however, remained unclear. Deleting these seemingly critical N-terminal sequences may disrupt intramolecular interactions within the protein chain which may affect the ability of  $\alpha$ S to achieve an amyloid competent conformation in which the NAC region is sufficiently exposed. Indeed, cryogenic electron microscopy (cryoEM) structures of  $\alpha$ S fibril polymorphs have identified residues in the P2 region as important stabilizers of its fibril cores. For example, residues<sup>47</sup>GVVHGVATVA<sup>56</sup> containing

uncharged glycine and alanine residues are shown to form the steric zipper between protofilaments.<sup>21</sup> Residues <sup>50</sup>HGVATV-AE<sup>57</sup> were also revealed by cryoEM to form a dimer interface between  $\alpha$ S subunits in the fibril structure, forming a parallel steric-zipper configuration,<sup>22,36</sup> while the P2 region is part of the core in all of the 48 currently solved amyloid structures of  $\alpha$ S.<sup>37</sup> Native IM-MS offers the potential to better understand how the conformational heterogeneity of  $\Delta\Delta$   $\alpha$ S correlates with its amyloid assembly propensity and whether removing the P1 and P2 regions which contain in total one positive lysine residue, the singular histidine residue present in  $\alpha$ S, and two negatively charged residues disrupts the overall charge balance of the  $\alpha$ S sequence.

*In vivo*,  $\alpha$ S is predominantly acetylated at the N-terminus.<sup>38</sup> More specifically, the composition of Lewy Body deposits has been shown to contain a high degree of N-terminally acetylated (NTA)  $\alpha$ S.<sup>39,40</sup> NTA of  $\alpha$ S has been shown to influence its membrane binding affinity through increased helicity of the N-terminal region, as well as to facilitate chaperone binding.<sup>11,41</sup>  $\alpha$ S *in vivo* is located in presynaptic nerve terminals in the brain. Calcium ions ( $\text{Ca}^{2+}$ ) are known to bind extensively to  $\alpha$ S at the C-terminal region,<sup>42,43</sup> they are essential for the transduction of electrical signals into chemical signals, but other metal ions have been shown to alter synaptic transmission.<sup>44,45</sup> Further to this, heavy metal ions have been linked to neurotoxicity and are markedly elevated in amyloid plaques deposited in the brain.<sup>45–47</sup> In its native environment,  $\alpha$ S will thus experience different physiological environments and conditions which could potentially alter the distribution of monomeric conformers and their propensity to aggregate into amyloid. Due to the high abundance of negatively charged residues in the C-terminal region of  $\alpha$ S, binding of positively charged ions is observed in this region (Figure 1a).<sup>24,25</sup> Binding of metal ions to residues in the C-terminal region will affect the charge distribution of  $\alpha$ S through neutralization of Glu and Asp residues, although precisely how interactions with different metal ions alters the monomeric conformational ensemble of  $\alpha$ S is unclear.

Here, the binding of divalent ions  $\text{Ca}^{2+}$ ,  $\text{Mn}^{2+}$ , and  $\text{Zn}^{2+}$  to N-terminally acetylated wild-type (WTNTA),  $\Delta\Delta$ NTA, and a C-terminally truncated variant, 119NTA  $\alpha$ S (Figure 1), has been observed through native MS, and the resultant effects on the conformational ensemble and amyloid assembly propensity have been investigated using native IM-MS, ThT fluorescence, and TEM, in order to correlate the conformational dynamics of  $\alpha$ S with amyloid formation. The results provide evidence which suggests that perturbing the charge distribution of  $\alpha$ S through metal ion binding, or sequence truncations, restricts the conformational freedom of the polypeptide chain and causes population shifts in the conformational ensemble, which has marked effects on the rates of amyloid assembly. Such compaction of monomeric  $\alpha$ S species may uncover the earliest stages of amyloid assembly at the monomer level, potentially identifying whether the enhancement of particular conformations predispose the amyloid propensity of  $\alpha$ S.

## MATERIALS AND METHODS

**Protein Expression and Purification.** Competent BL21 DE3 cells expressing NatB acetylase were prepared as follows. BL21 DE3 (Agilent) cells were transformed with the pNatB plasmid (Addgene 53613), and a single colony was used to inoculate a starter culture of LB media overnight at 37 °C, 200 rpm. The overnight culture was used to inoculate 500 mL LB

containing 25  $\mu\text{g}/\text{mL}$  chloramphenicol until an  $\text{OD}_{600}$  of 0.6 was reached. Cells were pelleted at 4500g for 5 min. Cells were resuspended in 30 mM potassium acetate, 10 mM  $\text{CaCl}_2$ , 50 mM  $\text{MnCl}_2$ , 100 mM  $\text{RbCl}$ , 15% (v/v) glycerol, pH 5.8. Cells were incubated on ice for 5 min before pelleting and further resuspension in 10 mM MOPS, 75 mM  $\text{CaCl}_2$ , 10 mM  $\text{RbCl}$ , 15% (v/v) glycerol, pH 6.5. Competent cells were stored at  $-80$  °C until used.

Competent NatB-BL21 DE3 cells were transformed with a pET23a plasmid encoding WT human full length  $\alpha$ S,  $\Delta\Delta$  or 119  $\alpha$ S to express both NatB and  $\alpha$ S for N-terminal acetylation. Expressed protein was purified by cell lysis in 25 mM Tris-HCl pH 8.0, 100  $\mu\text{g}/\text{mL}$  lysozyme, 50  $\mu\text{g}/\text{mL}$  PMSF, 1 mM benzamidine, and 20  $\mu\text{g}/\text{mL}$  DNase and homogenized using an IKA T 18 ULTRA-TURRAX homogenizer (IKA, Staufen, Germany). The lysate was heated to 80 °C for 10 min and then centrifuged at 35,000g for 30 min, 4 °C, followed by ammonium sulfate precipitation (50% w/v). The pellet containing  $\alpha$ S was diluted in 20 mM Tris-HCl, pH 8.0, and purified by anion exchange using a 350 mL Q-Sepharose fast flow anion-exchange column on an ÄKTA Prime (Cytiva, UK). Bound  $\alpha$ S was eluted in a gradient of 0–500 mM NaCl, in 20 mM Tris-HCl, pH 8.0, over a volume of 700 mL. Fractions containing  $\alpha$ S were dialyzed against 5  $\times$  5 L of 50 mM ammonium bicarbonate (3500 MWCO) at 4 °C and lyophilized. Freeze-dried protein was resuspended in 50 mM ammonium bicarbonate at 5 mg/mL and loaded onto a HiLoad 26/60 Superdex-75 column for size-exclusion chromatography. Fractions containing  $\alpha$ S were pooled and lyophilized.

**Kinetics of Amyloid Formation.** Kinetics of  $\alpha$ S amyloid formation were monitored in a 96-well, nonbinding, flat-bottom, half-area microplate (Corning, USA; 10438082) containing one Teflon polyball (1/8" diameter; Polysciences Europe, Eppelheim, Germany) per each well of sample. Samples of 100  $\mu\text{L}$  containing 100  $\mu\text{M}$   $\alpha$ S with 20  $\mu\text{M}$  Thioflavin T in 20 mM ammonium acetate, pH 7.5, were incubated at 37 °C shaking at 600 rpm in a FLUOstar omega plate reader (BMG Labtech, Ortenburg, Germany). Fluorescence intensity was measured by exciting at  $440 \pm 10$  nm and collecting emission at  $482 \pm 12$  nm using a bandpass filter. For experiments involving the addition of metal ions, zinc acetate, manganese acetate, or calcium acetate (Sigma Life Sciences, Germany) was added at a concentration of 2.5 mM (i.e., 25 fold excess over protein) per well. Results were blank-corrected using wells containing 20  $\mu\text{M}$  ThT in 20 mM ammonium acetate, pH 7.5, and normalized to the maximum fluorescence value of each curve.

**Negative Stain TEM.** A sample of 5  $\mu\text{L}$  was taken from the ThT plate at the end-point of each reaction, loaded onto a glow discharged (30s, Pelco Easi-glow), 400 mesh continuous carbon grid, and incubated for 2 min. The sample was blotted and washed twice with  $\text{H}_2\text{O}$  before being blotted and stained twice with 2% (w/v) uranyl acetate. Grids were imaged on a Tecnai F20 electron microscope (FEI) with a Ceta CCD detector (FEI) in the Astbury EM facility (University of Leeds), using a nominal magnification of 9600 $\times$  corresponding to a pixel size of 1.05 nm/pixel.

**Quantification of Fibril Yield.** Fibril yields were determined by pelleting 50  $\mu\text{L}$  of the end point of the ThT reaction at 100,000g (Optima TLX ultracentrifuge, Beckman Coulter, TLA 100 rotor) at 4 °C for 30 min, and the amount of protein in the sample, as well as an unclarified sample from the

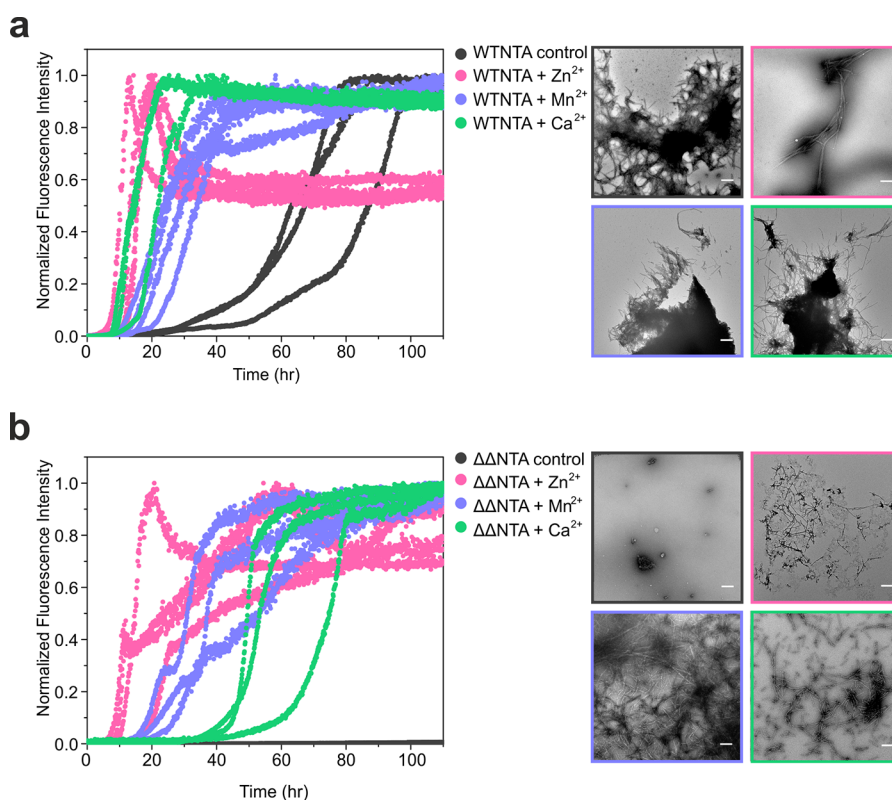


**Figure 2.** Metal ions increase the rate of WTNTA  $\alpha$ S amyloid assembly and switch on amyloid formation of  $\Delta\Delta$ NTA  $\alpha$ S. (a) Amyloid assembly of three replicates of WTNTA  $\alpha$ S (gray) alone and in the presence of a 25-fold molar excess of Zn<sup>2+</sup> (pink), Mn<sup>2+</sup> (purple), or Ca<sup>2+</sup> (green). Negative stain TEM images are shown as boxes (right) colored according to the respective ThT curves. All of the images were taken at the end of the ThT reactions using the same magnification. The scale bar corresponds to 300 nm in all images. (b) As in panel (a), but for  $\Delta\Delta$ NTA  $\alpha$ S.

reaction end point, was quantified by densitometry of sodium dodecyl sulfate–polyacrylamide gel electrophoresis (SDS–PAGE) gels. Tris-tricine buffered 30% (w/v) acrylamide:0.8% (w/v) bis(acrylamide) gels were stained with InstantBlue Coomassie/protein stain and imaged on an Alliance Q9 imager (Uvitec, Cambridge, UK). Band intensities were quantified using ImageJ 1.52a.

**Native IM-MS.** Native IM-MS experiments were performed on a Synapt G1 HD mass spectrometer (Waters Corporation, Wilmslow, UK) with traveling (T-wave) ion mobility and a nano-ESI source using in-house generated gold- and palladium-coated capillaries.  $\alpha$ S variants were analyzed at a concentration of 20  $\mu$ M, and spectra were collected with and without the addition of 500  $\mu$ M zinc acetate, manganese acetate, or calcium acetate (Sigma Life Sciences, Germany) at a ratio of 1:25  $\alpha$ S:metal ion. The unbound peak profiles for all three variants were taken from an external control without metal, since the unbound peak was sometimes not visible in spectra with a 25-fold excess of metal ion. MassLynx V4.1 (Waters Corporation, Wilmslow, UK) was used for data processing. Instrument parameters were set at capillary voltage 1.4 kV, source temperature 30 °C, sampling cone 18 V, extraction cone 1.0 V, trap collision energy 5.0 V, transfer collision energy 2.0 V, trap DC bias 30 V, IM wave velocity 300 m/s, and IM wave height 7.0 V. Gas pressures in the instrument were trap cell 0.0256 mbar and IM cell 0.36 mbar. The IM data was calibrated according to the Bush database<sup>49</sup> using denatured cytochrome c (charge states 13+ to 19+), myoglobin (charge states 15+ to 24+), and ubiquitin (charge states 7+ to 13+) at 10  $\mu$ M in 50% (v/v) acetonitrile, 0.1% (v/v) formic acid.

## RESULTS

**Divalent Metal Ions Increase the Rate of Amyloid Assembly.** To investigate how the addition of the metal ions Zn<sup>2+</sup>, Mn<sup>2+</sup>, and Ca<sup>2+</sup> affects the aggregation propensity of WTNTA  $\alpha$ S and  $\Delta\Delta$ NTA  $\alpha$ S, the rate of amyloid assembly was measured using ThT fluorescence (Figure 2a,b). The end points of the reaction (after 110 h) were imaged via negative stain TEM, and the percentage of pelletable material was determined through ultracentrifugation and quantitative analysis of the percent pelleted material by analysis using SDS–PAGE.

For these experiments, a 25-fold molar excess of metal ion: $\alpha$ S was used in order to saturate possible binding sites, following previous protocols.<sup>50</sup> The rate of ThT positive amyloid assembly for WTNTA  $\alpha$ S was accelerated when each of the three tested metal ions were added (Figure 2a). A significant decrease in the half time was observed, determined from  $t_{50}$  values which represent the time taken for each fluorescence signal to reach half of the plateau value calculated using AmyloFit 2.0.<sup>51</sup> This effect is most prominent in the presence of Zn<sup>2+</sup>, where the  $t_{50}$  is reduced from an average of  $64.4 \pm 18.8$  h to  $13.4 \pm 2.6$  h (Figure S1). All of the tested ions are found in presynaptic nerve terminals;<sup>45–47,52,53</sup> therefore, the amyloid assembly kinetics presented here could offer understandings of the behavior of  $\alpha$ S in its native environment. In the absence of metal ions, the variant  $\Delta\Delta$ NTA  $\alpha$ S does not assemble into ThT positive amyloid fibrils within 110 h (Figure 2b, Figure S1). The deletion of both the P1 and P2 regions might disrupt intramolecular interactions which are involved in the assembly of a partially compact structure on

pathway for amyloid assembly. Strikingly, the addition of  $Zn^{2+}$ ,  $Mn^{2+}$ , or  $Ca^{2+}$  all induced amyloid formation of  $\Delta\Delta$ NTA  $\alpha$ S, which otherwise does not assemble into amyloid on the time scale of these experiments (Figure 2b).

The results presented in Figure 2b suggest that metal ion binding could enable the formation of new amyloid-competent conformation(s) adopted by the monomer of  $\Delta\Delta$ NTA  $\alpha$ S or result in the enhancement in the population of a pre-existing amyloid-competent subpopulation. Similarly to the observations with WTNTA  $\alpha$ S,  $Zn^{2+}$  exerts the greatest effect on the rate of ThT positive amyloid assembly for  $\Delta\Delta$ NTA  $\alpha$ S, with  $Mn^{2+}$  less effective and  $Ca^{2+}$  having the smallest effect of the three metal ions tested. The resultant effect of each ion could arise through different binding stoichiometries or coordination sites resulting in different conformational shifts upon binding. The increase in the rate of amyloid formation could be a result of neutralization of the negatively charged C-terminal region of  $\alpha$ S due to coordination of divalent metal ions, which disrupts the overall charge distribution across the protein sequence. This charge distribution could be a fine-tuned feature of  $\alpha$ S, and disruption would result in exposure of the NAC region. The conformational properties of  $\alpha$ S, therefore, were next explored by native IM-MS to gain insight into how  $\alpha$ S conformational flexibility could influence amyloid propensity and the rate of assembly.

**Native IM-MS Compaction of Low Charge States Occurs When Metal Ions Bind  $\alpha$ S.** Ion mobility MS can detect subtle changes in compaction or expansion of dynamic protein conformations which may not already be visible from native charge state distributions (CSD). The CSD of WTNTA  $\alpha$ S in the presence of  $Zn^{2+}$  (Figure 3; the protein in the absence of metal ion is shown in Figure S2) shows a multimodal distribution, with surprisingly low charge states (5+ to 9+) present for an IDP indicating the presence of compact conformations.<sup>54,55</sup>

Binding of divalent metal ions to the intrinsically disordered ensemble of  $\alpha$ S may result in significant structural changes due to metal ion coordination, most likely by aspartic acid and glutamic acid residues in the protein sequence. Analysis of WTNTA  $\alpha$ S using native IM-MS results in a conformational fingerprint which contains four distinct conformations at the 8+ charge state, which was selected to represent the greatest conformational diversity of all charge states in the unbound state (Figure 4a), consistent with previous analysis of unacetylated WT  $\alpha$ S.<sup>50</sup> When metal ions  $Zn^{2+}$ ,  $Mn^{2+}$ , or  $Ca^{2+}$  are added, a multimodal CSD is still observed (Figure 3, Figure S3) and a clear compaction of the polypeptide chain occurs (Figure 4a). Strikingly, in the case of  $\Delta\Delta$ NTA  $\alpha$ S, a similar compaction with divalent metal ions is seen (Figure 4b, Figure S4) for the 7+ charge state. We selected the 7+ charge state here as it has equivalent charge density on its proportionally smaller solvent-accessible surface compared with the 8+ charge state for the larger WTNTA  $\alpha$ S. It also exhibited the greatest conformational diversity in the apo form, involving three distinct conformations for this deletion construct (Figure 4b). In particular, the CSD (Figure 3b) and compaction effect (based on the relative population of each species observed in the IM-MS CCS data) is strongest in the presence of  $Zn^{2+}$  (Figure S5), which also resulted in the fastest amyloid assembly kinetics.

When studying conformational changes by IM-MS, it is important to consider all charge states from the broad, multimodal distribution, as this reflects the entirety of the

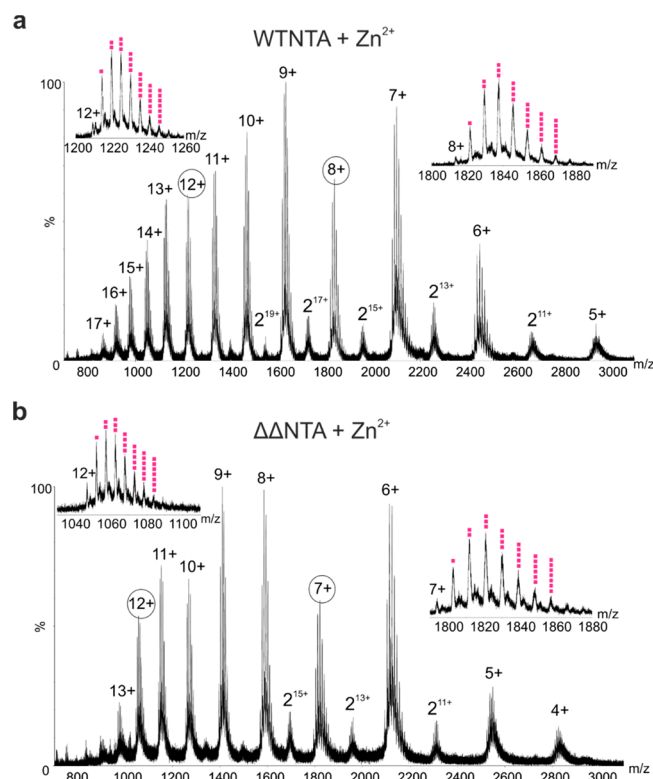


**Figure 3.** Native nESI mass spectra showing  $Zn^{2+}$  binding to WTNTA and  $\Delta\Delta$ NTA  $\alpha$ S. (a) Native nESI mass spectrum of WTNTA  $\alpha$ S bound to  $Zn^{2+}$  ions. Insets show up to seven  $Zn^{2+}$  bound to the 8+ and 12+ charge states (pink squares). (b) As in panel (a) but for  $\Delta\Delta$ NTA  $\alpha$ S bound to  $Zn^{2+}$ . Insets show up to seven metals bound to the 7+ and 12+ charge states. The protein concentration was 20  $\mu$ M in 20 mM ammonium acetate, pH 7.5, at a molar ratio of 1:25  $\alpha$ S: $Zn^{2+}$ . Dimers are indicated by “2”. Spectra were acquired using a Synapt G1 instrument.

conformational ensemble.<sup>54</sup> The native nESI mass spectra of WTNTA and  $\Delta\Delta$ NTA  $\alpha$ S show binding of  $Zn^{2+}$  to all charge states to a similar extent at the molar excess used (Figure 3a,b). Since  $Zn^{2+}$  exhibited the greatest accelerator effect on amyloid formation and greatest effect on the extent of compaction with metal ion addition for both variants, this ion was selected for analysis of CCS effects. The CCS fingerprint for each charge state is plotted in Figure 5a–c for WTNTA  $\alpha$ S and Figure 5d–f for  $\Delta\Delta$ NTA  $\alpha$ S, each unbound, bound to one  $Zn^{2+}$ , and bound to four  $Zn^{2+}$ . Investigating the effect of  $Zn^{2+}$  binding on the CCS values reveals that structural remodeling of  $\alpha$ S primarily occurs at low charge states. Low charge states (6+ to 9+ for WTNTA and 6+ to 8+ for  $\Delta\Delta$ NTA  $\alpha$ S) represent compact conformations with a smaller solvent accessible surface area (SASA), reducing the amount of protonation during native ESI. These compact conformations become even more compact upon  $Zn^{2+}$  binding, whereas ions with higher charge states reflecting a larger SASA (more extended conformations) exhibit no such striking change in CCS in response to binding of one or four  $Zn^{2+}$  ions.  $Zn^{2+}$  exhibits specific conformational effects on particular  $\alpha$ S conformations, likely due to facilitated coordination of binding due to the close proximity of negatively charged residues in the C-terminal region, together with the presence of some negatively charged residues, and transition metal coordinating methionine and His50 residues in the N-terminal region (Figure 1b).

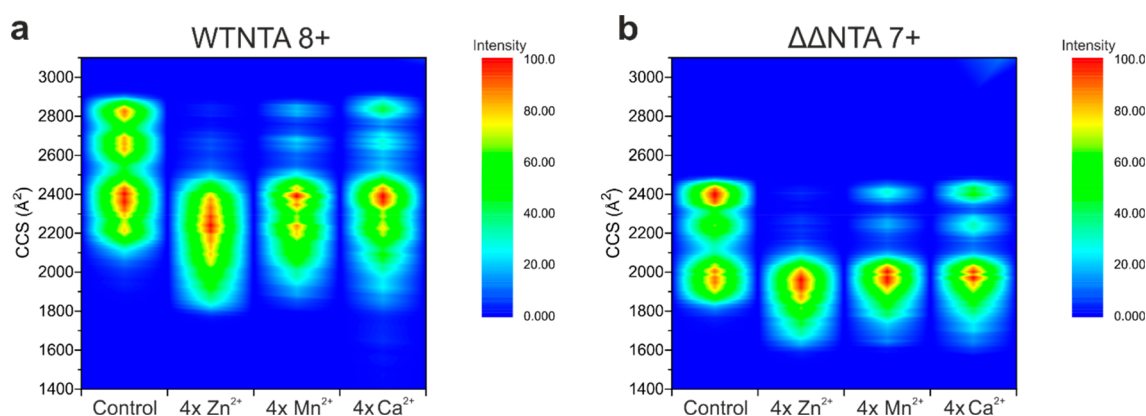


**Figure 4.** Native nESI-IM mass spectra showing compaction of WTNTA and  $\Delta\Delta$ NTA  $\alpha$ S when metal ions bind. (a) CCS fingerprints of the 8+ charge state of WTNTA  $\alpha$ S either alone calculated using an external control or bound to four ions of either  $\text{Zn}^{2+}$ ,  $\text{Mn}^{2+}$ , or  $\text{Ca}^{2+}$ . (b) CCS fingerprints of the  $\Delta\Delta$ NTA  $\alpha$ S 7+ charge state either alone calculated using an external control or bound to four ions of either  $\text{Zn}^{2+}$ ,  $\text{Mn}^{2+}$ , or  $\text{Ca}^{2+}$ . All spectra were acquired using a protein concentration of 20  $\mu\text{M}$  in 20 mM ammonium acetate, pH 7.5. A 25-fold molar excess of metal ion was added. CCS values were calculated using ATDs extracted from MassLynx 4.1 software and calibrated as described in the Methods section.

**C-Terminal Truncation Variant 119NTA of  $\alpha$ S Retains Metal Ion Binding.** Within Lewy bodies, around 15% of total  $\alpha$ S is estimated to be truncated within the C-terminal region, resulting in different length variants of  $\alpha$ S which are naturally occurring and may act as seeds.<sup>56</sup> From *in vivo* studies of Lewy bodies, truncations at residues 119 and 122 are most prevalent.<sup>57–59</sup> Primary sites of metal ion binding have been localized to residues Asp121, Asn122, and Glu123 through heteronuclear single quantum coherence (HSQC) NMR experiments.<sup>24</sup> It is thought that this region in the C-terminal domain might offer a favorable orientation of moieties for metal ion coordination governed by electrostatic interactions. The C-terminal region of full length  $\alpha$ S has been suggested to exert a protective effect against aggregation due to the large number of negative charges which could form long-range interactions with the N-terminal region that shield the hydrophobic NAC region from nucleation events.<sup>26</sup> Truncation of the C-terminal sequence has been shown in several studies to increase the rate of  $\alpha$ S amyloid assembly, which we were also able to observe (Figure 6).<sup>60–62</sup> Here, we explored whether divalent metal ions could exert a similar effect on the truncated, acetylated variant 119 of acceleration of amyloid formation despite some key divalent metal ion binding sites being deleted.

The effect of adding  $\text{Zn}^{2+}$ ,  $\text{Mn}^{2+}$ , or  $\text{Ca}^{2+}$  to 119NTA  $\alpha$ S on amyloid formation is shown in Figure 6. While  $\text{Ca}^{2+}$  results in comparable kinetics to the rate of amyloid assembly in the absence of metal ions, both  $\text{Mn}^{2+}$  and  $\text{Zn}^{2+}$  induce faster kinetics, despite the fact that the truncated variant forms amyloid already 5-fold more rapidly than WTNTA  $\alpha$ S (Figure S6) and lacks two aspartic acid and six glutamic acid residues of the WT sequence. Native IM-MS of 119NTA  $\alpha$ S [which displayed a multimodal charge state distribution in the absence of a metal ion (Figure S7)] shows that although eight D/E residues have been removed from the sequence, all three types of metal ions still bind to the protein sequence (Figure 7a and Figure S8), and all three ions shift the ensemble to populate compact conformations with the greatest conformational shift again observed in the presence of  $\text{Zn}^{2+}$  (Figure 7 and Figure S9). The N-terminal region, however, is unaffected by this deletion, with seven aspartic acid residues and one glutamic acid residue. These negative charges also offer essential binding sites for metal ions, which may have been overlooked in

previous studies using very low concentrations of ions.<sup>24</sup> Additionally to these residues, the N-terminal region contains two methionine residues which can act as interaction sites for transition metals.<sup>25</sup> Furthermore, His50, which is removed in the  $\Delta\Delta$ NTA variant of  $\alpha$ S, may act as a compensatory metal ion binding site for 119NTA  $\alpha$ S.

## DISCUSSION

$\alpha$ S is an IDP, and its conformational behavior is known to be affected by divalent metal ion binding.<sup>24,25,50,63,64</sup> Native IM-MS has shown that WTNTA  $\alpha$ S populates four major conformational families at the 8+ charge state, consistent with previous data.<sup>43,50</sup> We use CCS measurements to demonstrate that there is a clear and consistent link between the compaction of monomeric  $\alpha$ S at the 8+ charge state for WTNTA  $\alpha$ S and the 7+ charge state for  $\Delta\Delta$ NTA  $\alpha$ S with an increased rate of amyloid formation, possibly indicating that key species in the ensemble are compacted such that they are more competent to form amyloid. How the properties of species observed in the gas phase relate to those in solution (e.g., their hydrodynamic radius, or the formation of intra- or intermolecular contacts) will require further analyses using solution-based assays. For example, it is well-known that hydrophobic contacts are diminished in the absence of water, while hydrogen bonding and electrostatic interactions are enhanced.<sup>65</sup> Such effects are especially important to consider for weak complexes, such as the early oligomers in amyloid formation, and dynamically disordered monomeric proteins, such as IDPs. Importantly, however, previous analyses comparing gas phase and solution properties of IDPs have shown that the ESI process does not have a substantial effect on structure and that IM-MS CCS can report accurately on their solution phase properties.<sup>66</sup> Backed up with solution phase assays, therefore, MS-based methods provide a unique power for understanding the structure, populations, and stabilities of proteins in complex mixtures, as exemplified here for the effects of different metal ions in the self-assembly of  $\alpha$ S. CCS values obtained also enable us to compare different deletion variants of  $\alpha$ S in the absence of metal ions to determine the effect of the protein sequence and distribution of charged residues on the conformational behavior of the apo state. We show that WTNTA  $\alpha$ S visits more conformational states than  $\Delta\Delta$ NTA  $\alpha$ S overall as shown in Figure 5, some of

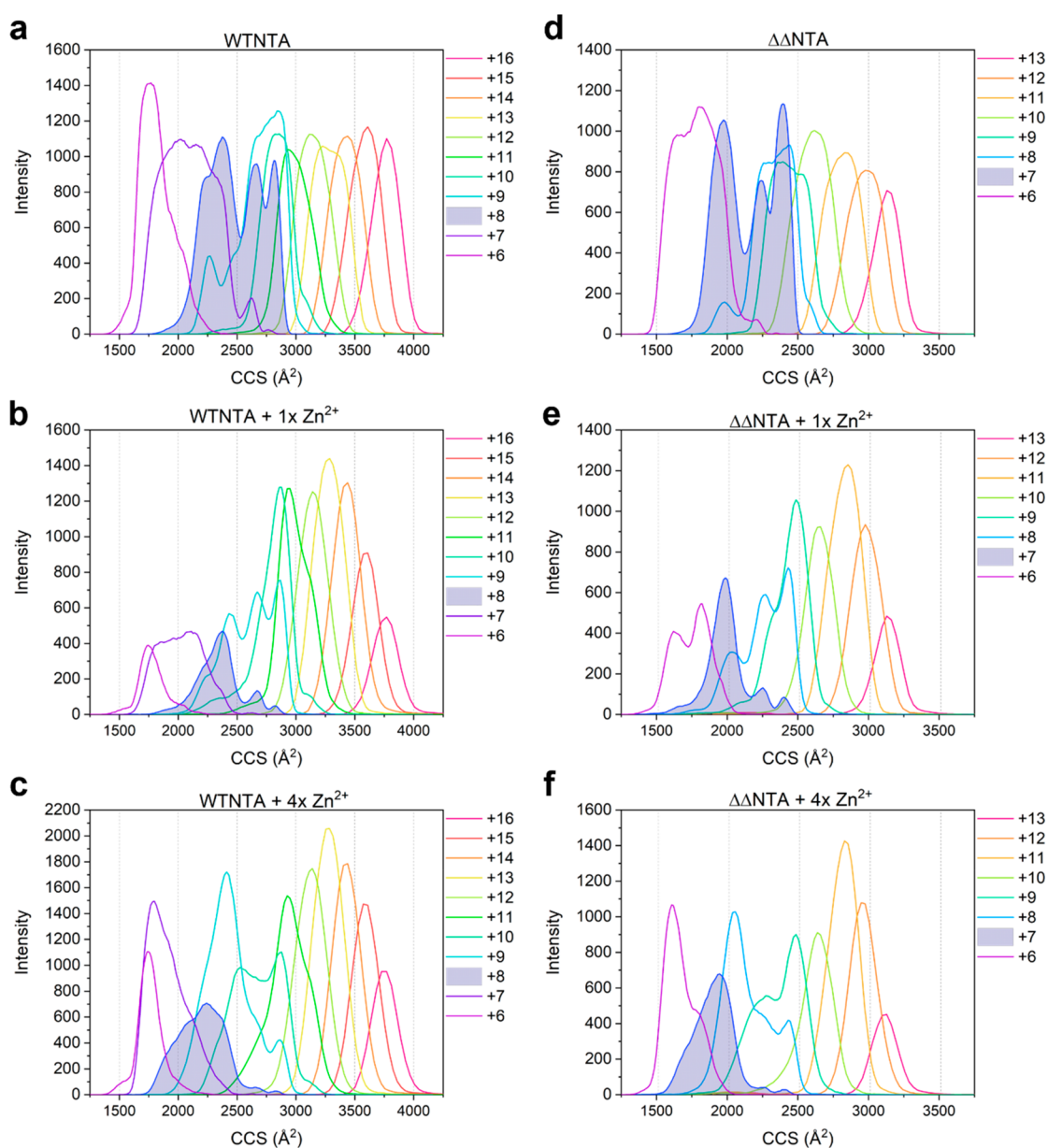


**Figure 5.** Metal ions selectively modulate compaction of low charge states of the  $\alpha$ S variants. CCS fingerprints of the entire charge state distribution (6+ to 16+) of (a) WTNTA  $\alpha$ S alone, (b) WTNTA  $\alpha$ S bound to one  $\text{Zn}^{2+}$ , and (c) WTNTA  $\alpha$ S bound to four  $\text{Zn}^{2+}$  ions. The 8+ charge state is highlighted by shading in each plot. The spectra show that lower charge states of WTNTA  $\alpha$ S become more compact when  $\text{Zn}^{2+}$  binds, with higher charge states being relatively unaffected by  $\text{Zn}^{2+}$  binding. CCS fingerprints of the entire charge state distribution (6+ to 13+) of (d)  $\Delta\Delta$ NTA  $\alpha$ S alone, (e)  $\Delta\Delta$ NTA  $\alpha$ S bound to one  $\text{Zn}^{2+}$ , and (f)  $\Delta\Delta$ NTA  $\alpha$ S bound to four  $\text{Zn}^{2+}$  ions. The 7+ charge state is highlighted in d–f where a similar effect can be observed to WTNTA  $\alpha$ S. ATDs were extracted using MassLynx 4.1.

which presumably are competent to form amyloid. Shifting the conformational ensemble to populate species with smaller CCS combined with charge neutralization from divalent metal ion binding appear to have a key regulatory effect in increasing the rate of ThT positive amyloid assembly. Carija et al. used a disulfide link strategically placed between residues Val71 and Thr92 to lock the monomeric structure of WT  $\alpha$ S into the Greek-key motif of  $\alpha$ S amyloid fibrils. This compacted monomer resulted in reduced amyloid formation, highlighting the importance of conformational flexibility and dynamic conformational exchange in the early stages of assembly to generate the amyloid fold.<sup>67</sup>

There is a hierarchal reduction in the  $t_{50}$  of amyloid formation for WTNTA  $\alpha$ S, whereby  $\text{Zn}^{2+}$  is the most effective,

followed by  $\text{Mn}^{2+}$  and  $\text{Ca}^{2+}$ . A study using laser ablation-inductively coupled plasma-MS (LA-ICP-MS) of homogenized human olfactory bulb samples from PD patients identified that  $\text{Zn}^{2+}$  was present at 10–200  $\mu\text{g/g}$  concentrations, colocalized with aggregates of phosphorylated  $\alpha$ S, while  $\text{Mn}^{2+}$  was found at trace levels (less than 1  $\mu\text{g/g}$  on average). Zinc in particular was thought to contribute to Lewy body pathology in PD through oxidative stress, having a mostly pathological role.<sup>47</sup> Physiological  $\text{Ca}^{2+}$  concentrations can vary from tens of nM to several hundreds of  $\mu\text{M}$ , depending on whether neuronal cells are in a resting state or undergoing depolarization during an action potential.<sup>68</sup> With a  $K_D$  of 21  $\mu\text{M}$  for  $\alpha$ S with  $\text{Ca}^{2+}$ , it is clear that  $\alpha$ S will interact with  $\text{Ca}^{2+}$  in the physiological, cellular context.<sup>42</sup> Lautenschläger et al. showed a relationship

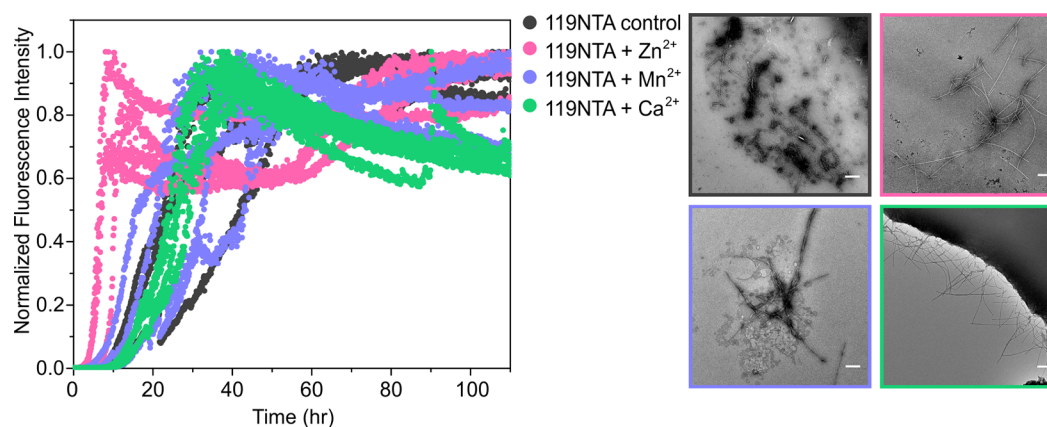


**Figure 6.** Metal ion binding modulates the rate of 119NNTA  $\alpha$ S amyloid assembly. Amyloid assembly of 119NNTA  $\alpha$ S (black) alone or in the presence of  $Zn^{2+}$  (pink),  $Mn^{2+}$  (purple), or  $Ca^{2+}$  (green). Negative stain TEM images taken at the end of the reactions are shown (right) with box outlines colored according to the respective ThT curves. The scale bar corresponds to 300 nm for all images.

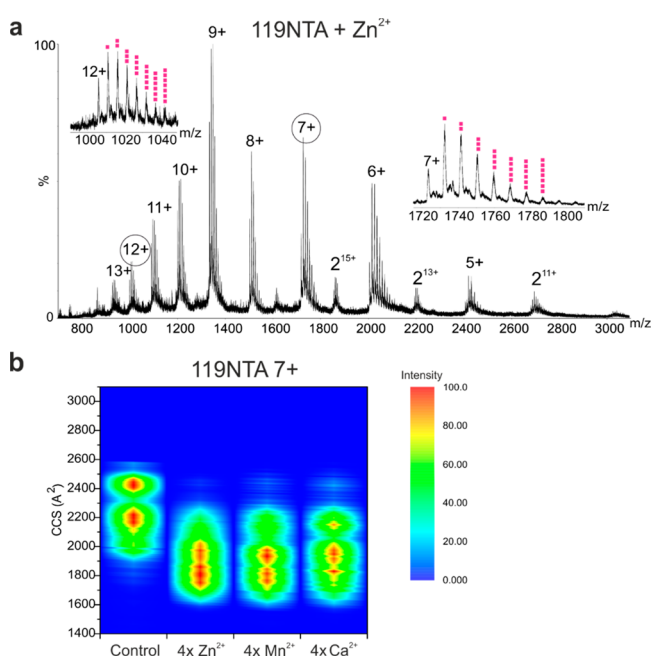


**Figure 7.** Native nESI-IM-MS spectra show compaction of 119NNTA  $\alpha$ S when metal ions bind. (a) Native nESI mass spectrum of 119NNTA  $\alpha$ S bound to  $Zn^{2+}$ . Insets show up to seven  $Zn^{2+}$  ions bound to the 7+ and 12+ charge states (pink squares) (b) CCS fingerprints of 119NNTA  $\alpha$ S 7+ charge state alone or bound to four ions of either  $Zn^{2+}$ ,  $Mn^{2+}$ , or  $Ca^{2+}$ . All spectra were acquired using a protein concentration of 20  $\mu$ M in 20 mM ammonium acetate, pH 7.5. Spectra with metal ions present were acquired in the presence of 500 mM ion acetate conjugate. All spectra were acquired on a Synapt G1 instrument. CCS values were calculated using ATDs extracted from MassLynx 4.1.

between C-terminal  $Ca^{2+}$  binding and  $\alpha$ S synaptic vesicle interactions.<sup>42</sup> Moreover, the presence of  $Ca^{2+}$  ions increased the affinity of  $\alpha$ S to synaptic vesicle membranes, which resulted in increased clustering of vesicles.<sup>42</sup> The presence of metal ions influences the behavior of  $\alpha$ S within cells and may elude to mechanisms hidden in synucleopathies. This study provides further molecular detail into the resulting effects on  $\alpha$ S when metal ions bind.

*In vivo*, binding of other small molecules or proteins such as chaperones may offer a protective effect against pathological

structural remodelling of  $\alpha$ S. Molecules such as dopamine are known to also bind to the C-terminal region of  $\alpha$ S, and binding results in extension of the protein chain which offers a protective effect, switching off aggregation into the amyloid.<sup>69</sup> Additionally, chaperones such as Hsp70 and Hsp40 are known to interact with the N-terminal region of  $\alpha$ S, protecting it from amyloid assembly.<sup>70,71</sup> *In vivo*, chaperone binding could offer a protective effect which counteracts the effects of metal ion binding.

Introducing the  $\Delta\Delta$  variant to the  $\alpha$ S sequence through removal of P1 and P2 sequences switches off the potential for  $\alpha$ S to assemble into amyloid by altering the long-range interactions necessary to induce an amyloid-competent conformation.<sup>34</sup> Even though these sequences remove critical interaction sites, we show that  $\Delta\Delta$ NNTA  $\alpha$ S still remains conformationally dynamic by native IM-MS (Figure 4b and Figure S2b). However, this variant populates three distinct conformations at the 7+ charge state wherein the largest CCS conformation (most extended) is the most intensely populated, whereas WTNTA  $\alpha$ S populates four CCS conformations (at the 8+ charge state) with the population intensity weighted toward the compact conformations. Strikingly, when divalent metal ions are present, the  $\Delta\Delta$ NNTA  $\alpha$ S amyloid assembly potential is re-established, and this effect consistently correlates with compaction, reinforcing the correlation between chain compaction and the rate of amyloid formation.

As metal ion binding is believed to be located primarily to negatively charged Asp and Glu residues in the C-terminal region of  $\alpha$ S, physiologically relevant C-terminally truncated variants of  $\alpha$ S may inform on the necessity of charge neutralization in this process, or whether compaction alone is the primary driver. Additionally, transition metals can also interact with methionine and histidine residues, potentially recruiting the N-terminal region of  $\alpha$ S; however, this is not known for  $Ca^{2+}$ .<sup>24,25,42</sup> We repeated native IM-MS and ThT kinetics on a variant of  $\alpha$ S truncated at residue 119 (1–119), which was also acetylated at the N-terminus (119NNTA) in the absence and presence of metal ions. Native IM-MS in Figure 7 shows that the +7 charge state of 119NNTA  $\alpha$ S variant populates fewer conformational states than  $\Delta\Delta$ NNTA  $\alpha$ S, where the intensity is split between one extended conformation and one compact conformation with some additional compact CCS values represented as weaker intensity below the intense compact conformation CCS. Interestingly, despite half of the

putative C-terminal metal binding region being removed in 119NTA  $\alpha$ S, an almost comparable number of ions still bind to the protein, with 1–2 fewer binding events on average compared to WTNTA  $\alpha$ S. These binding events still result in CCS compaction and faster amyloid assembly kinetics. These results imply that the N-terminal region must also be important for metal ion binding and that the presence of a compact conformation is compatible with metal ion binding. The seven aspartic acid residues and single glutamic acid residue within the N-terminal region may become preferential to divalent metal ions when the C-terminal region is truncated. His50 may offer an essential binding mechanism which anchors metal ions by coordination with the C-terminal region creating a seemingly looped structure of  $\alpha$ S.

Compact conformations may offer a preferential, higher stability orientation for metal ion binding as the close proximity of negatively charged amino acids creates a binding pocket when the C-terminus folds backward to interact with the N-terminus. Ions can create a coordination network between these negatively charged amino acids which pull the structure into a tighter, more compact conformation which may also result in increasingly rigid conformations, depicted from low charge states in the CCS evaluation in Figure 5. CCS compaction has been observed previously in the case of increased numbers of  $\text{Ca}^{2+}$  binding to calmodulin, established by IM-MS.<sup>72</sup> As for the higher charge states, these extended conformations still bind to  $\text{Zn}^{2+}$  and other metal ions; however, due to the distance between negatively charged residues, metal ions presumably cannot hold distant residues together, resulting in no significant observable conformational change.

## CONCLUSION

We hypothesize that the conformational ensemble of the monomeric state predisposes  $\alpha$ -synuclein's functional and amyloid-forming behavior. The charge distribution across the sequence of the protein might be naturally fine-tuned in a way that prevents the rapid onset of amyloid assembly, tipping the toxicity versus function of  $\alpha$ S away from toxicity. Binding of metal ions or other ligands such as small molecules, lipids, or membranes could bias  $\alpha$ S toward amyloid-prone conformations, resulting in the rapid assembly of toxic oligomers and ultimately amyloid fibrils which are associated with disease.

Further information regarding the exact binding sites of metal ions to WTNTA  $\alpha$ S, as well as  $\Delta\Delta$ NTA  $\alpha$ S and 119NTA  $\alpha$ S, will help to elucidate the exact molecular rearrangement that the  $\alpha$ S protein chain undergoes when metal ions bind. Binding sites can be mapped using techniques such as native top-down electron-capture or transfer dissociation (ECD/ETD) tandem mass spectrometry (MS/MS) which fragments the backbone of intact proteins while maintaining noncovalent ligand binding. In addition, residue- and region-specific details of the conformational changes that  $\alpha$ S undergoes in the presence of metal ion binding could be unravelled using techniques such as NMR or cross-linking MS to identify specific intraprotein interactions that stabilize compact conformations or studies using techniques such as smFRET analysis of population shifts using probes placed at relevant sites on the protein sequence.<sup>73</sup> With powerful MS methods adding to a fast-growing structural toolbox, our next goal is to target the structural gap in protein aggregation pathways between monomer and fibril, by elucidating structural intermediates such as oligomeric and phase-

separated states and identify potential targets for pharmaceutical intervention.

## ASSOCIATED CONTENT

### Supporting Information

The Supporting Information is available free of charge at <https://pubs.acs.org/doi/10.1021/jasms.2c00379>.

$t_{50}$  values and fibril yields for WTNTA and  $\Delta\Delta$ NTA  $\alpha$ S amyloid assembly as well as 119NTA  $\alpha$ S amyloid assembly, native ESI mass spectra showing unbound WTNTA and  $\Delta\Delta$ NTA  $\alpha$ S as well as  $\text{Mn}^{2+}$  and  $\text{Ca}^{2+}$  binding to WTNTA  $\alpha$ S and  $\Delta\Delta$ NTA  $\alpha$ S, native IM mass spectra showing compaction of WTNTA,  $\Delta\Delta$ NTA  $\alpha$ S, and 119NTA  $\alpha$ S when different numbers of  $\text{Zn}^{2+}$  ions bind, and native ESI mass spectra showing 119NTA  $\alpha$ S in the absence of metal ions as well as  $\text{Mn}^{2+}$  and  $\text{Ca}^{2+}$  binding to 119NTA  $\alpha$ S (PDF)

## AUTHOR INFORMATION

### Corresponding Author

Frank Sobott – Astbury Centre for Structural Molecular Biology, School of Molecular and Cellular Biology, Faculty of Biological Sciences, University of Leeds, Leeds LS2 9JT, United Kingdom; [orcid.org/0000-0001-9029-1865](https://orcid.org/0000-0001-9029-1865); Email: [f.sobott@leeds.ac.uk](mailto:f.sobott@leeds.ac.uk)

### Authors

Emily J. Byrd – Astbury Centre for Structural Molecular Biology, School of Molecular and Cellular Biology, Faculty of Biological Sciences, University of Leeds, Leeds LS2 9JT, United Kingdom

Martin Wilkinson – Astbury Centre for Structural Molecular Biology, School of Molecular and Cellular Biology, Faculty of Biological Sciences, University of Leeds, Leeds LS2 9JT, United Kingdom

Sheena E. Radford – Astbury Centre for Structural Molecular Biology, School of Molecular and Cellular Biology, Faculty of Biological Sciences, University of Leeds, Leeds LS2 9JT, United Kingdom; [orcid.org/0000-0002-3079-8039](https://orcid.org/0000-0002-3079-8039)

Complete contact information is available at: <https://pubs.acs.org/doi/10.1021/jasms.2c00379>

### Author Contributions

E.J.B. expressed and purified proteins, prepared samples, and performed ThT and native IM-MS experiments. M.W. performed TEM experiments. S.E.R. and F.S. developed the ideas and supervised the project. All authors contributed to the preparation of the manuscript.

### Notes

The authors declare no competing financial interest.

## ACKNOWLEDGMENTS

We thank the members of our research groups for helpful discussions. We thank Antonio Calabrese (University of Leeds) for helpful discussion regarding MS. E.J.B. is supported by BBSRC (BB/M011151/1). All MS experiments were performed with instrumentation from the Biomolecular Mass Spectrometry Facility (University of Leeds), with the Synapt HDMS mass spectrometer funded by BBSRC (BB/E012558/1). EM experiments were performed on instruments in the Astbury EM facility (University of Leeds) which is funded by the University of Leeds and the Wellcome Trust (108466/Z/

15/Z). S.E.R. is the grateful recipient of a Royal Society Research Professorship (RSRP/R1/211057), and M.W. is funded by the UK Medical Research Council (MR/T011149/1). Finally, we thank James Ault and Nasir Khan for excellent technical support and the colleagues in the Radford laboratory for helpful discussions while preparing this work.

## REFERENCES

- (1) Meade, R. M.; Fairlie, D. P.; Mason, J. M. Alpha-synuclein structure and Parkinson's disease – lessons and emerging principles. *Mol. Neurodegener* **2019**, *14*, 29.
- (2) Holdorff, B. Friedrich Heinrich Lewy (1885–1950) and His Work. *J. Hist. Neurosci* **2002**, *11*, 19–28.
- (3) Mor, D. E.; Ugras, S. E.; Daniels, M. J.; Ischiropoulos, H. Dynamic structural flexibility of  $\alpha$ -synuclein. *Nuerobiol. Dis* **2016**, *88*, 66–74.
- (4) Spillantini, M. G.; Schmidt, M. L.; Lee, V. M. Y.; Trojanowski, J. Q.; Jakes, R.; Goedert, M.  $\alpha$ -Synuclein in Lewy bodies. *Nature* **1997**, *388*, 839–840.
- (5) Mahul-Mellier, A.-L.; Burtscher, J.; Maharjan, N.; Weerens, L.; Croisier, M.; Kuttler, F.; Leleu, M.; Knott, G. W.; Lashuel, H. A. The process of Lewy body formation, rather than simply  $\alpha$ -synuclein fibrillization, is one of the major drivers of neurodegeneration. *Proc. Natl. Acad. Sci. U.S.A.* **2020**, *117*, 4971–4982.
- (6) Gai, W. P.; Yuan, H. X.; Li, X. Q.; Power, J. T. H.; Blumbergs, P. C.; Jensen, P. H. In Situ and in Vitro Study of Colocalization and Segregation of  $\alpha$ -Synuclein, Ubiquitin, and Lipids in Lewy Bodies. *Exp. Neurol.* **2000**, *166*, 324–333.
- (7) den Hartog Jager, W. A. Sphingomyelin in Lewy Inclusion Bodies in Parkinson's Disease. *Arch. Neurol* **1969**, *21*, 615–619.
- (8) Shahmoradian, S. H.; Lewis, A. J.; Genoud, C.; Hench, J.; Moors, T. E.; Navarro, P. P.; Castaño-Diez, D.; Schweighauser, G.; Graff-Meyer, A.; Goldie, K. N.; Sütterlin, R.; Huisman, E.; Ingrassia, A.; Gier, Y. d.; Rozemuller, A. J. M.; Wang, J.; Paepe, A. D.; Emy, J.; Staempfli, A.; Hoenschmeyer, J.; Großerüschkamp, F.; Niedieker, D.; El-Mashtoly, S. F.; Quadri, M.; Van Ijcken, W. F. J.; Bonifati, V.; Gerwert, K.; Bohrmann, B.; Frank, S.; Britschgi, M.; Stahlberg, H.; Van de Berg, W. D. J.; Lauer, M. E. Lewy pathology in Parkinson's disease consists of crowded organelles and lipid membranes. *Nat. Neurosci* **2019**, *22*, 1099–1109.
- (9) Törnquist, M.; Michaels, T. C. T.; Sanagavarapu, K.; Yang, X.; Meisl, G.; Cohen, S. I. A.; Knowles, T. P. J.; Linse, S. Secondary nucleation in amyloid formation. *Chem. Commun.* **2018**, *54*, 8667–8684.
- (10) Fusco, G.; De Simone, A.; Gopinath, T.; Vostrikov, V.; Vendruscolo, M.; Dobson, C. M.; Veglia, G. Direct observation of the three regions in  $\alpha$ -synuclein that determine its membrane-bound behaviour. *Nat. Commun.* **2014**, *5*, 3827.
- (11) Runfola, M.; De Simone, A.; Vendruscolo, M.; Dobson, C. M.; Fusco, G. The N-terminal Acetylation of  $\alpha$ -Synuclein Changes the Affinity for Lipid Membranes but not the Structural Properties of the Bound State. *Sci. Rep* **2020**, *10*, 204.
- (12) Burré, J.; Sharma, M.; Südhof, T. C.  $\alpha$ -Synuclein assembles into higher-order multimers upon membrane binding to promote SNARE complex formation. *Proc. Natl. Acad. Sci. U.S.A.* **2014**, *111*, E4274–E4283.
- (13) Cabin, D. E.; Shimazu, K.; Murphy, D.; Cole, N. B.; Gottschalk, W.; McIlwain, K. L.; Orrison, B.; Chen, A.; Ellis, C. E.; Paylor, R.; Lu, B.; Nussbaum, R. L. Synaptic Vesicle Depletion Correlates with Attenuated Synaptic Responses to Prolonged Repetitive Stimulation in Mice Lacking  $\alpha$ -Synuclein. *J. Neurosci* **2002**, *22*, 8797–8807.
- (14) Soper, J. H.; Roy, S.; Stieber, A.; Lee, E.; Wilson, R. B.; Trojanowski, J. Q.; Burd, C. G.; Lee, V. M. Y.  $\alpha$ -Synuclein-induced Aggregation of Cytoplasmic Vesicles in *Saccharomyces cerevisiae*. *Mol. Biol. Cell* **2008**, *19*, 1093–1103.
- (15) Diao, J.; Burré, J.; Vivona, S.; Cipriano, D. J.; Sharma, M.; Kyoung, M.; Südhof, T. C.; Brunker, A. T. Native  $\alpha$ -synuclein induces clustering of synaptic-vesicle mimics via binding to phospholipids and synaptobrevin-2/VAMP2. *eLife* **2013**, *2*, No. 1.
- (16) Bartels, T.; Ahlstrom, L. S.; Leftin, A.; Kamp, F.; Haass, C.; Brown, M. F.; Beyer, K. The N-Terminus of the Intrinsically Disordered Protein  $\alpha$ -Synuclein Triggers Membrane Binding and Helix Folding. *Biophys. J.* **2010**, *99*, 2116–2124.
- (17) Lee, S. J. C.; Lee, J. W.; Choi, T. S.; Jin, K. S.; Lee, S.; Ban, C.; Kim, H. I. Probing Conformational Change of Intrinsically Disordered  $\alpha$ -Synuclein to Helical Structures by Distinctive Regional Interactions with Lipid Membranes. *Anal. Chem.* **2014**, *86*, 1909–1916.
- (18) Moons, R.; van der Wekken-de Bruijne, R.; Maudsley, S.; Lemièrre, F.; Lambeir, A.-M.; Sobott, F. Effects of Detergent on  $\alpha$ -Synuclein Structure: A Native MS-Ion Mobility Study. *Int. J. Mol. Sci.* **2020**, *21*, 7884.
- (19) Salveson, P. J.; Spencer, R. K.; Nowick, J. S. X-ray Crystallographic Structure of Oligomers Formed by a Toxic  $\beta$ -Hairpin Derived from  $\alpha$ -Synuclein: Trimers and Higher-Order Oligomers. *J. Am. Chem. Soc.* **2016**, *138*, 4458–4467.
- (20) Giasson, B. I.; Murray, I. V. J.; Trojanowski, J. Q.; Lee, V. M. Y. A Hydrophobic Stretch of 12 Amino Acid Residues in the Middle of  $\alpha$ -Synuclein Is Essential for Filament Assembly. *J. Biol. Chem.* **2001**, *276*, 2380–2386.
- (21) Li, B.; Ge, P.; Murray, K. A.; Sheth, P.; Zhang, M.; Nair, G.; Sawaya, M. R.; Shin, W. S.; Boyer, D. R.; Ye, S.; Eisenberg, D. S.; Zhou, Z. H.; Jiang, L. Cryo-EM of full-length  $\alpha$ -synuclein reveals fibril polymorphs with a common structural kernel. *Nat. Commun.* **2018**, *9*, 3609.
- (22) Guerrero-Ferreira, R.; Taylor, N. M.; Mona, D.; Ringler, P.; Lauer, M. E.; Riek, R.; Britschgi, M.; Stahlberg, H. Cryo-EM structure of alpha-synuclein fibrils. *eLife* **2018**, *7*, No. 1.
- (23) Tuttle, M. D.; Comellas, G.; Nieuwkoop, A. J.; Covell, D. J.; Berthold, D. A.; Kloepper, K. D.; Courtney, J. M.; Kim, J. K.; Barclay, A. M.; Kendall, A.; Wan, W.; Stubbs, G.; Schwieters, C. D.; Lee, V. M. Y.; George, J. M.; Rienstra, C. M. Solid-state NMR structure of a pathogenic fibril of full-length human  $\alpha$ -synuclein. *Nat. Struct. Mol. Biol.* **2016**, *23*, 409–415.
- (24) Binolfi, A.; Rasia, R. M.; Bertocini, C. W.; Ceolin, M.; Zweckstetter, M.; Griesinger, C.; Jovin, T. M.; Fernández, C. O. Interaction of  $\alpha$ -Synuclein with Divalent Metal Ions Reveals Key Differences: A Link between Structure, Binding Specificity and Fibrillation Enhancement. *J. Am. Chem. Soc.* **2006**, *128*, 9893–9901.
- (25) Wongkongkathep, P.; Han, J. Y.; Choi, T. S.; Yin, S.; Kim, H. I.; Loo, J. A. Native Top-Down Mass Spectrometry and Ion Mobility MS for Characterizing the Cobalt and Manganese Metal Binding of  $\alpha$ -Synuclein Protein. *J. Am. Soc. Mass. Spectrom* **2018**, *29*, 1870–1880.
- (26) Hoyer, W.; Cherny, D.; Subramaniam, V.; Jovin, T. M. Impact of the Acidic C-Terminal Region Comprising Amino Acids 109–140 on  $\alpha$ -Synuclein Aggregation in Vitro. *Biochemistry* **2004**, *43*, 16233–16242.
- (27) Dedmon, M. M.; Lindorff-Larsen, K.; Christodoulou, J.; Vendruscolo, M.; Dobson, C. M. Mapping Long-Range Interactions in  $\alpha$ -Synuclein using Spin-Label NMR and Ensemble Molecular Dynamics Simulations. *J. Am. Chem. Soc.* **2005**, *127*, 476–477.
- (28) Brodie, N. I.; Popov, K. I.; Petrotchenko, E. V.; Dokholyan, N. V.; Borchers, C. H. Conformational ensemble of native  $\alpha$ -synuclein in solution as determined by short-distance crosslinking constraint-guided discrete molecular dynamics simulations. *PLoS Comput. Biol.* **2019**, *15*, e1006859–e1006859.
- (29) Chen, J.; Zaer, S.; Drori, P.; Zamel, J.; Joron, K.; Kalisman, N.; Lerner, E.; Dokholyan, N. V. The structural heterogeneity of alpha-synuclein is governed by several distinct subpopulations with interconversion times slower than milliseconds. *Structure* **2021**, *29*, 1048.
- (30) Fusco, G.; Chen, S. W.; Williamson, P. T. F.; Cascella, R.; Perni, M.; Jarvis, J. A.; Cecchi, C.; Vendruscolo, M.; Chiti, F.; Cremades, N.; Ying, L.; Dobson, C. M.; De Simone, A. Structural basis of membrane disruption and cellular toxicity by alpha-synuclein oligomers. *Science* **2017**, *358*, 1440–1443.

- (31) Nelson, R.; Sawaya, M. R.; Balbirnie, M.; Madsen, A. Ø.; Riekel, C.; Grothe, R.; Eisenberg, D. Structure of the cross- $\beta$  spine of amyloid-like fibrils. *Nature* **2005**, *435*, 773–778.
- (32) Sawaya, M. R.; Sambashivan, S.; Nelson, R.; Ivanova, M. I.; Sievers, S. A.; Apostol, M. I.; Thompson, M. J.; Balbirnie, M.; Wiltzius, J. J. W.; McFarlane, H. T.; Madsen, A. Ø.; Riekel, C.; Eisenberg, D. Atomic structures of amyloid cross- $\beta$  spines reveal varied steric zippers. *Nature* **2007**, *447*, 453–457.
- (33) Beveridge, R.; Calabrese, A. N. Structural Proteomics Methods to Interrogate the Conformations and Dynamics of Intrinsically Disordered Proteins. *Front. Chem.* **2021**, *9*, 1.
- (34) Doherty, C. P. A.; Ulapec, S. M.; Maya-Martinez, R.; Good, S. C.; Makepeace, J.; Khan, G. N.; van Oosten-Hawle, P.; Radford, S. E.; Brockwell, D. J. A short motif in the N-terminal region of  $\alpha$ -synuclein is critical for both aggregation and function. *Nat. Struct. Mol. Biol.* **2020**, *27*, 249–259.
- (35) Ulapec, S. M.; Maya-Martinez, R.; Byrd, E. J.; Dewison, K. M.; Xu, Y.; Willis, L. F.; Sobott, F.; Heath, G. R.; van Oosten Hawle, P.; Buchman, V. L.; Radford, S. E.; Brockwell, D. J. Single residue modulators of amyloid formation in the N-terminal P1-region of  $\alpha$ -synuclein. *Nat. Commun.* **2022**, *13*, 4986.
- (36) Li, Y.; Zhao, C.; Luo, F.; Liu, Z.; Gui, X.; Luo, Z.; Zhang, X.; Li, D.; Liu, C.; Li, X. Amyloid fibril structure of  $\alpha$ -synuclein determined by cryo-electron microscopy. *Cell. Res.* **2018**, *28*, 897–903.
- (37) Sawaya, M. R.; Hughes, M. P.; Rodriguez, J. A.; Riek, R.; Eisenberg, D. S. The expanding amyloid family: Structure, stability, function, and pathogenesis. *Cell* **2021**, *184*, 4857–4873.
- (38) Trexler, A. J.; Rhoades, E. N-terminal acetylation is critical for forming  $\alpha$ -helical oligomer of  $\alpha$ -synuclein. *Protein Sci.* **2012**, *21*, 601–605.
- (39) Anderson, J. P.; Walker, D. E.; Goldstein, J. M.; de Laat, R.; Banducci, K.; Caccavello, R. J.; Barbour, R.; Huang, J.; Kling, K.; Lee, M.; Diep, L.; Keim, P. S.; Shen, X.; Chataway, T.; Schlossmacher, M. G.; Seubert, P.; Schenk, D.; Sinha, S.; Gai, W. P.; Chilcote, T. J. Phosphorylation of Ser-129 Is the Dominant Pathological Modification of  $\alpha$ -Synuclein in Familial and Sporadic Lewy Body Disease. *J. Biol. Chem.* **2006**, *281*, 29739–29752.
- (40) Öhrfelt, A.; Zetterberg, H.; Andersson, K.; Persson, R.; Secic, D.; Brinkmalm, G.; Wallin, A.; Mulugeta, E.; Francis, P. T.; Vanmechelen, E.; Aarsland, D.; Ballard, C.; Blennow, K.; Westman-Brinkmalm, A. Identification of Novel  $\alpha$ -Synuclein Isoforms in Human Brain Tissue by using an Online NanoLC-ESI-FTICR-MS Method. *Neurochem. Res.* **2011**, *36*, 2029–2042.
- (41) Maltsev, A. S.; Ying, J.; Bax, A. Impact of N-Terminal Acetylation of  $\alpha$ -Synuclein on Its Random Coil and Lipid Binding Properties. *Biochemistry* **2012**, *51*, 5004–5013.
- (42) Lautenschläger, J.; Stephens, A. D.; Fusco, G.; Ströhl, F.; Curry, N.; Zacharopoulou, M.; Michel, C. H.; Laine, R.; Nespovitaya, N.; Fantham, M.; Pinotsi, D.; Zago, W.; Fraser, P.; Tandon, A.; St George-Hyslop, P.; Rees, E.; Phillips, J. J.; De Simone, A.; Kaminski, C. F.; Schierle, G. S. K. C-terminal calcium binding of  $\alpha$ -synuclein modulates synaptic vesicle interaction. *Nat. Commun.* **2018**, *9*, 712.
- (43) Stephens, A. D.; Zacharopoulou, M.; Moons, R.; Fusco, G.; Seetaloo, N.; Chiki, A.; Woodhams, P. J.; Mela, I.; Lashuel, H. A.; Phillips, J. J.; De Simone, A.; Sobott, F.; Schierle, G. S. K. Extent of N-terminus exposure by altered long-range interactions of monomeric  $\alpha$ -synuclein determines its aggregation propensity. *Nat. Commun.* **2020**, *11*, 2820.
- (44) Mattson, M. P. Calcium and neurodegeneration. *Aging Cell* **2007**, *6*, 337–350.
- (45) Lermyte, F.; Everett, J.; Brooks, J.; Bellingieri, F.; Billimoria, K.; Sadler, P. J.; O'Connor, P. B.; Telling, N. D.; Collingwood, J. F. Emerging Approaches to Investigate the Influence of Transition Metals in the Proteinopathies. *Cells* **2019**, *8*, 1231.
- (46) Finefrock, A. E.; Bush, A. I.; Doraiswamy, P. M. Current Status of Metals as Therapeutic Targets in Alzheimer's Disease. *J. Am. Geriatr. Soc.* **2003**, *51*, 1143–1148.
- (47) Gardner, B.; Dieriks, B. V.; Cameron, S.; Mendis, L. H. S.; Turner, C.; Faull, R. L. M.; Curtis, M. A. Metal concentrations and distributions in the human olfactory bulb in Parkinson's disease. *Sci. Rep.* **2017**, *7*, 10454.
- (48) Brown, D. R. Metal binding to alpha-synuclein peptides and its contribution to toxicity. *Biochem. Biophys. Res. Commun.* **2009**, *380*, 377–381.
- (49) Bush, M. F.; Hall, Z.; Giles, K.; Hoyes, J.; Robinson, C. V.; Ruotolo, B. T. Collision Cross Sections of Proteins and Their Complexes: A Calibration Framework and Database for Gas-Phase Structural Biology. *Anal. Chem.* **2010**, *82*, 9557–9565.
- (50) Moons, R.; Konijnenberg, A.; Mensch, C.; Van Elzen, R.; Johannessen, C.; Maudsley, S.; Lambeir, A.-M.; Sobott, F. Metal ions shape  $\alpha$ -synuclein. *Sci. Rep.* **2020**, *10*, 16293.
- (51) Meisl, G.; Kirkegaard, J. B.; Arosio, P.; Michaels, T. C. T.; Vendruscolo, M.; Dobson, C. M.; Linse, S.; Knowles, T. P. J. Molecular mechanisms of protein aggregation from global fitting of kinetic models. *Nat. Protoc.* **2016**, *11*, 252–272.
- (52) Sadiq, S.; Ghazala, Z.; Chowdhury, A.; Büsselberg, D. Metal Toxicity at the Synapse: Presynaptic, Postsynaptic, and Long-Term Effects. *J. Toxicol.* **2012**, *2012*, 132671.
- (53) Santner, A.; Uversky, V. N. Metalloproteomics and metal toxicology of  $\alpha$ -synuclein. *Metallomics* **2010**, *2*, 378–392.
- (54) Santambrogio, C.; Natalello, A.; Brocca, S.; Ponzini, E.; Grandori, R. Conformational Characterization and Classification of Intrinsically Disordered Proteins by Native Mass Spectrometry and Charge-State Distribution Analysis. *Proteomics* **2019**, *19*, 1800060.
- (55) Grandori, R.; Santambrogio, C.; Brocca, S.; Invernizzi, G.; Lotti, M. Electrospray-ionization mass spectrometry as a tool for fast screening of protein structural properties. *Biotechnol. J.* **2009**, *4*, 73–87.
- (56) Levitan, K.; Chereau, D.; Cohen, S. I. A.; Knowles, T. P. J.; Dobson, C. M.; Fink, A. L.; Anderson, J. P.; Goldstein, J. M.; Millhauser, G. L. Conserved C-Terminal Charge Exerts a Profound Influence on the Aggregation Rate of  $\alpha$ -Synuclein. *J. Mol. Biol.* **2011**, *411*, 329–333.
- (57) Sorrentino, Z. A.; Giasson, B. I. The emerging role of  $\alpha$ -synuclein truncation in aggregation and disease. *J. Biol. Chem.* **2020**, *295*, 10224–10244.
- (58) Liu, C.-W.; Giasson, B. I.; Lewis, K. A.; Lee, V. M.; DeMartino, G. N.; Thomas, P. J. A Precipitating Role for Truncated  $\alpha$ -Synuclein and the Proteasome in  $\alpha$ -Synuclein Aggregation: implications for pathogenesis of Parkinson disease. *J. Biol. Chem.* **2005**, *280*, 22670–22678.
- (59) Farzadfard, A.; Pedersen, J. N.; Meisl, G.; Somavarapu, A. K.; Alam, P.; Goksøyr, L.; Nielsen, M. A.; Sander, A. F.; Knowles, T. P. J.; Pedersen, J. S.; Otzen, D. E. The C-terminal tail of  $\alpha$ -synuclein protects against aggregate replication but is critical for oligomerization. *Commun. Biol.* **2022**, *5*, 123.
- (60) Crowther, R. A.; Jakes, R.; Spillantini, M. G.; Goedert, M. Synthetic filaments assembled from C-terminally truncated  $\alpha$ -synuclein. *FEBS Lett.* **1998**, *436*, 309–312.
- (61) Serpell, L. C.; Berriman, J.; Jakes, R.; Goedert, M.; Crowther, R. A. Fiber diffraction of synthetic  $\alpha$ -synuclein filaments shows amyloid-like cross- $\beta$  conformation. *Proc. Natl. Acad. Sci. U.S.A.* **2000**, *97*, 4897–4902.
- (62) Li, W.; West, N.; Colla, E.; Pletnikova, O.; Troncoso, J. C.; Marsh, L.; Dawson, T. M.; Jäkälä, P.; Hartmann, T.; Price, D. L.; Lee, M. K. Aggregation promoting C-terminal truncation of  $\alpha$ -synuclein is a normal cellular process and is enhanced by the familial Parkinson's disease-linked mutations. *Proc. Natl. Acad. Sci. U.S.A.* **2005**, *102*, 2162–2167.
- (63) Mason, R. J.; Paskins, A. R.; Dalton, C. F.; Smith, D. P. Copper Binding and Subsequent Aggregation of  $\alpha$ -Synuclein Are Modulated by N-Terminal Acetylation and Ablated by the H50Q Missense Mutation. *Biochemistry* **2016**, *55*, 4737–4741.
- (64) Han, J. Y.; Choi, T. S.; Kim, H. I. Molecular Role of Ca<sup>2+</sup> and Hard Divalent Metal Cations on Accelerated Fibrillation and Interfibrillar Aggregation of  $\alpha$ -Synuclein. *Sci. Rep.* **2018**, *8*, 1895.

(65) Bich, C.; Baer, S.; Jecklin, M. C.; Zenobi, R. Probing the Hydrophobic Effect of Noncovalent Complexes by Mass Spectrometry. *J. Am. Soc. Mass. Spectrom.* **2010**, *21*, 286–289.

(66) Stuchfield, D.; Barran, P. Unique insights to intrinsically disordered proteins provided by ion mobility mass spectrometry. *Curr. Opin. Chem. Biol.* **2018**, *42*, 177–185.

(67) Carija, A.; Pinheiro, F.; Pujols, J.; Brás, I. C.; Lázaro, D. F.; Santambrogio, C.; Grandori, R.; Outeiro, T. F.; Navarro, S.; Ventura, S. Biasing the native  $\alpha$ -synuclein conformational ensemble towards compact states abolishes aggregation and neurotoxicity. *Redox Biol.* **2019**, *22*, 101135.

(68) Everett, J.; Collingwood, J. F.; Tjendana-Tjhin, V.; Brooks, J.; Lermlyte, F.; Plascencia-Villa, G.; Hands-Portman, I.; Dobson, J.; Perry, G.; Telling, N. D. Nanoscale synchrotron X-ray speciation of iron and calcium compounds in amyloid plaque cores from Alzheimer's disease subjects. *Nanoscale* **2018**, *10*, 11782–11796.

(69) Illes-Toth, E.; Dalton, C. F.; Smith, D. P. Binding of Dopamine to Alpha-Synuclein is Mediated by Specific Conformational States. *J. Am. Soc. Mass. Spectrom.* **2013**, *24*, 1346–1354.

(70) Burmann, B. M.; Gerez, J. A.; Matečko-Burmann, I.; Campioni, S.; Kumari, P.; Ghosh, D.; Mazur, A.; Aspholm, E. E.; Sulskis, D.; Wawrzyniuk, M.; Bock, T.; Schmidt, A.; Rüdiger, S. G. D.; Riek, R.; Hiller, S. Regulation of  $\alpha$ -synuclein by chaperones in mammalian cells. *Nature* **2020**, *577*, 127.

(71) Tao, J.; Berthet, A.; Citron, Y. R.; Tsiolaki, P. L.; Stanley, R.; Gestwicki, J. E.; Agard, D. A.; McConlogue, L. Hsp70 chaperone blocks  $\alpha$ -synuclein oligomer formation via a novel engagement mechanism. *J. Biol. Chem.* **2021**, *296*, 100613.

(72) Wyttenbach, T.; Grabenauer, M.; Thalassinos, K.; Scrivens, J. H.; Bowers, M. T. The Effect of Calcium Ions and Peptide Ligands on the Relative Stabilities of the Calmodulin Dumbbell and Compact Structures. *J. Phys. Chem. B* **2010**, *114*, 437–447.

(73) Cawood, E. E.; Karamanos, T. K.; Wilson, A. J.; Radford, S. E. Visualizing and trapping transient oligomers in amyloid assembly pathways. *Biophys. Chem.* **2021**, *268*, 106505.

## Recommended by ACS

### Potential Protective Function of $A\beta_{42}$ Monomer on Tauopathies

Amber L. H. Gray, Thanh D. Do, *et al.*

JANUARY 24, 2023  
JOURNAL OF THE AMERICAN SOCIETY FOR MASS SPECTROMETRY

READ 

### DJ-1 Molecular Chaperone Activity Depresses Tau Aggregation Propensity through Interaction with Monomers

Daniela Jimenez-Harrison, Jeff Kuret, *et al.*

FEBRUARY 22, 2023  
BIOCHEMISTRY

READ 

### Determining the Location of the $\alpha$ -Synuclein Dimer Interface Using Native Top-Down Fragmentation and Isotope Depletion-Mass Spectrometry

Kiani Jeacock, David J. Clarke, *et al.*

MARCH 28, 2023  
JOURNAL OF THE AMERICAN SOCIETY FOR MASS SPECTROMETRY

READ 

### Amyloid Fibril Formation of Arctic Amyloid- $\beta$ 1–42 Peptide is Efficiently Inhibited by the BRICHOS Domain

Xueying Zhong, Gefei Chen, *et al.*

JULY 25, 2022  
ACS CHEMICAL BIOLOGY

READ 

Get More Suggestions >